Fabrication of hierarchical porous iron oxide films utilizing the Kirkendall effect†

Lizhi Zhang,*[a] Jimmy C. Yu,*[b] Zhi Zheng[b] and Cheuk Wan Leung[b]

Received (in Cambridge, UK) 21st February 2005, Accepted 24th March 2005
First published as an Advance Article on the web 12th April 2005
DOI: 10.1039/b502526e

Hierarchical porous iron oxide films with different morphologies have for the first time been fabricated through hydrothermal reactions between an iron substrate and iodine powder in water or ethanol, which can be explained by a mechanism analogous to the Kirkendall effect.

It was reported by Kirkendall decades ago that the interface between copper and zinc in brass could move at an elevated temperature because the two elements diffused at different rates.[1] A common result from this effect is the formation of porosity in the lower-melting component side of the diffusion couple.[2] The pore formation during the growth of metal oxide films can be explained by the fast outward diffusion of cations through the oxide layer accompanying by an inward flow of vacancies to the vicinity of the metal–oxide interface.[3] While metallurgists try to suppress the Kirkendall effect to prevent void formation in alloys, chemists take advantage of the phenomenon to prepare nanomaterials of unusual morphology. For example, ZnO "Dandelions" as well as hollow nanocrystals of cobalt oxides and chalcogenides have been fabricated *via* modified Kirkendall processes.[2,3] In this communication, we demonstrate that the Kirkendall effect can also be utilized to fabricate hierarchical porous transition metal oxide films on metal substrates.

Porous solids have excellent adsorptive properties which possess numerous applications in catalysis and separation.[4] Calculations and simulations have demonstrated that, if diffusion limitations are to exist in a catalyst with unisized nanopores (micro- or small-mesopores), the catalytic process would occur more efficiently in materials with hierarchical pore size distribution in nano- and macro-scales.[5] These have motivated the design of hierarchical porous materials including silica,[6] titania,[7] zicornia,[8] zeolite,[9] aluminosilicate,[10] carbon monoliths,[11] single-wall carbon nanotube fibers,[12] V_2O_5 battery electrode,[13] noble metals,[14] calcium carbonate,[15] manganese oxide,[16] ZnO,[17] iron oxide.[18] In most of these preparations, various organic templates (*e.g.* surfactants, diatom, bacteria, emulsion) are needed to build the hierarchical porous scaffolds, followed by thermal treatment to remove the templates, resulting in consumption of energy and environmental pollution.

Iron oxides are important catalytic and magnetic materials. Representative iron oxides include α-Fe_2O_3, γ-Fe_2O_3 and Fe_3O_4. α-Fe_2O_3 has the corundum structure, while the other two have the spinel structure. γ-Fe_2O_3 and Fe_3O_4 are metastable in the oxidative atmosphere, so they will be oxidized to α-Fe_2O_3 by heating above 400 °C. Iron oxides are widely applied in catalysis such as styrene synthesis,[19] photocatalytic production of hydrogen and oxygen by water splitting,[20] removal of carbon monoxide,[21] selective oxidation of NH_3 and reduction of NO by NH_3,[22] reduction of aromatic nitro compounds with hydrazine hydrate,[23] catalytic conversion of methane into aromatic hydrocarbons,[24] *etc*. It is expected that the catalytic efficiencies should be greatly enhanced if hierarchical porous iron oxides could be applied in these reactions as we have proven that hierarchical porous titania showed much enhanced photocatalytic activity.[7] Very recently, Jiao and Bruce used decylamine as a template to prepare ordered mesoporous Fe_2O_3 with microporous wall.[25] In their synthesis, deceylamine template was removed with excess ethanol. Recently, there are several interesting reports of growing chalcogenide or oxide nanostructures on metal foils.[17a,26] Here we report for the first time that hierarchical porous α-Fe_2O_3 or Fe_3O_4 films with different morphologies can selectively be grown through hydrothermal reactions between an iron substrate and iodine powder in water or ethanol without any organic templates. The formation of porous iron oxide films can be explained by a mechanism analogous to the Kirkendall effect. Moreover, our method can be extended to grow hierarchical porous cobalt on cobalt substrate, indicating its generality for the synthesis of hierarchical porous metal oxide films.

Fig. 1 shows the representative X-ray diffraction (XRD) patterns of films grown in different media. Apart from two peaks arising from (110) and (200) planes of iron substrate, all other peaks in the patterns of the rust-colored samples synthesized in water can be indexed to a hexagonal phase [space group: $R\bar{3}c$ (167)] of α-Fe_2O_3 (Hematite, JCPDS file No. 87-1166). It seems

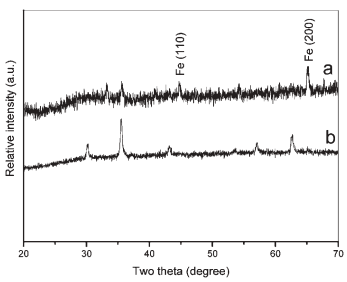

Fig. 1 The representative XRD patterns of the resulting films grown in different media. a) in water, b) in ethanol.

† Electronic supplementary information (ESI) available: details of preparation and characterization procedure of hierarchical porous iron oxide films, EDX spectra of iron oxide films formed at different stages, SEM images of films synthesized in the absence of iodine, TEM and SEM images of hierarchical porous cobalt oxide films, and nitrogen absorption–desorption isotherms. See http://www.rsc.org/suppdata/cc/b5/b502526e/

*zhanglz@mail.ccnu.edu.cn (Lizhi Zhang)
jimyu@cuhk.edu.hk (Jimmy C. Yu)

that the crystal size of the resulting α-Fe_2O_3 is very small according to the XRD pattern. In the case that ethanol was the reaction medium, the XRD pattern of the resulting black-colored film can be indexed to a face-centered cubic phase [space group: $Fd\bar{3}m$ (227)] of Fe_3O_4 (Magnetite, JCPDS file No. 85-1436). The crystal size of Fe_3O_4 is significantly larger than that of α-Fe_2O_3. No peak of iron substrate is observed because Fe_3O_4 film is thicker than that of α-Fe_2O_3 film.

The morphology of the resulting films was investigated by a scanning electron microscopy (SEM). Fig. 2 shows the SEM images of iron oxides with different morphologies. Spherical particles of micrometer size were observed in the α-Fe_2O_3 film grown in water in the presence of iodine (inset of Fig. 2a). The high-magnification SEM image reveals numerous needle- or flake-like particles on the surfaces of the spheres (Fig. 2a). Macropores or large mesopores are formed between these needles or flakes. When water was replaced by ethanol in the synthesis, the surface of the resulting Fe_3O_4 film became smoother (inset of Fig. 2b). Macropores in the range of 0.5 to 10 micrometers are found between oriented sheets on the substrate (Fig. 2b). The thickness of the sheets is from about 200 nm to 1 micrometer. It was found that the addition of surfactants could modify the morphologies of the films. When cetyltrimethylammonium bromide (CTAB) or NaAOT was introduced to the reaction system, more abundant and uniform nanosheets were produced on the substrates (Fig. 2c–e).

The microstructures of the resulting iron oxide films are further investigated by transmission electron microscopy. Panels a and c of Fig. 3 confirm the sheet-like structure of iron oxides. It is interesting to find that there are plenty of wormhole-like nanopores in each sheet, suggesting that the resulting iron oxide films are of hierarchical porous structure. The aggregation and/or assembly of the nanosheets give rise to macropores, while the aggregation of the primary nanoparticles produces nanopores in the nanosheets. The HRTEM images (Fig. 3b and 3d) show the crystal sizes of α-Fe_2O_3 and Fe_3O_4 are about 3 and 10 nm, respectively. The size of α-Fe_2O_3 is obviously smaller than that of Fe_3O_4. This is in agreement with the XRD results. Results of energy-dispersive X-ray (EDX) analysis confirm that the final films consist of only iron and oxygen. However, iron, oxygen, and iodine could be detected in the films grown at early stages during hydrothermal reaction (ESI†).

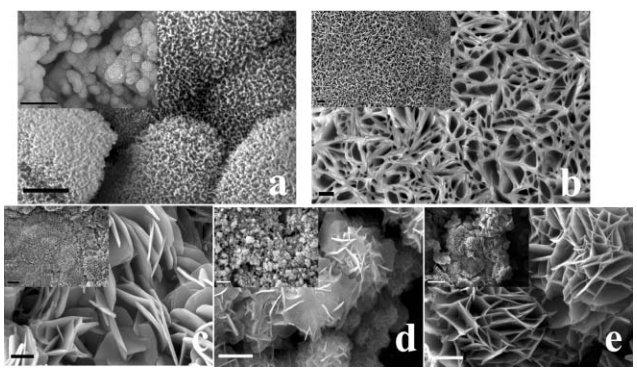

Fig. 2 Various iron oxide films grown under different conditions. a) 0.2% I_2 aqueous solution at 160 °C, b) 2% I_2 ethanolic solution at 180 °C, c) 2% I_2 aqueous solution with 0.4 g CTAB at 180 °C, d) 2% I_2 ethanolic solution with 0.4 g CTAB at 180 °C, e) 2% I_2 aqueous solution with 0.4 g NaAOT at 180 °C. Scale bar in a, b, c, d, e: 2 μm; Scale bar in inset of a, b, c, d, e: 20 μm.

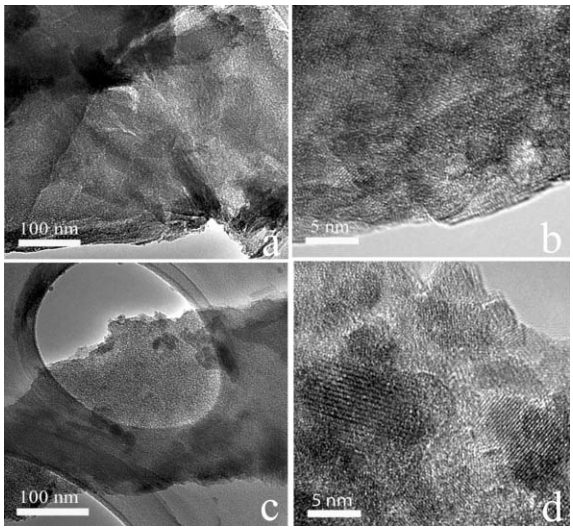

Fig. 3 TEM and HRTEM images of iron oxide nanosheets. a, b) α-Fe_2O_3, c, d) Fe_3O_4.

Nitrogen sorption characterizations further substantiate the hierarchical porous structures of iron oxide films. The Brunauer–Emmett–Teller (BET) specific surface areas of the resulting iron oxide films are in the range from 100 to 336 $m^3\ g^{-1}$.

The formation of hierarchical porous iron oxide films is attributed to the introduction of iodine, which create fast reaction–diffusion rates because of its high reactivity.[27] The participation of iodine in the formation of hierarchical porous films is supported by the existence of iodine in the films grown at early stages during hydrothermal reaction (ESI†). It is also found that no hierarchical pores can be obtained without the addition of iodine, even in the presence of a surfactant CTAB (ESI†). The selective growth of α-Fe_2O_3 and Fe_3O_4 in water and ethanol is thought to be relative to different reaction ways of iodine with iron in different solvents. It is known that the solubility of iodine in water is much smaller than that in ethanol, while iodine can disproportionally react with water as follows.[27]

$$6\ I_2 + 6\ H_2O \rightarrow 6\ HI + 6\ HOI \quad (1)$$

$$6\ HOI \rightarrow 3\ I_2 + 3\ H_2O + 3/2\ O_2 \quad (2)$$

Meanwhile, iron may also react with water or iodine under hydrothermal condition:

$$Fe + 2\ H_2O \rightarrow Fe^{2+} + 2\ OH^- + H_2 \quad (3)$$

$$Fe + I_2 \rightarrow FeI_2 \quad (4)$$

According to Wren *et al.*,[28] reaction (4) is the fastest one. They found that the fast reaction between gaseous iodine and iron in stainless steel produce randomly oriented FeI_2 scales through migration of iron to the surface and subsequently react with oxygen in air to form FeI_xO_y (a mixture of FeI_2, FeIO and iron oxide).[28] In our study, α-Fe_2O_3 was found to be the final product. This is because under an oxidizing reaction condition, α-Fe_2O_3 is more thermodynamically stable than FeI_2 and it is also the most

stable form of iron oxide. The final reaction is postulated as follows.

$$4\ FeI_2 + 3\ O_2 \rightarrow 2\ Fe_2O_3 + 2\ I_2 \quad (5)$$

Therefore, iodine takes the role of a catalyst in our study, different from its transportation role in the synthesis of $PbSnS_3$ nanorods and other iodine compounds.[29] The presence of iodine increases the oxidation rate of iron, resulting in a high-speed outward diffusion of iron cations and an inward flow of fast-moving vacancies to the vicinity of the oxide–metal interface. Thus, macropores are formed through coalescence of the vacancies on iron substrate during the formation of oriented FeI_2 nanosheets. As FeI_2 nanosheets are formed by the fast reactions, they have many defect sites. These defects together with volume changes during their subsequent oxidation to Fe_2O_3 would create the nanopores in the nanosheets. In comparison, the reactions in ethanol are not as complex as those in water. Through the iodine-catalyzed fast oxidation of iron shown in reaction (4), FeI_2 nanosheets are first formed on an iron substrate in ethanol. Their aggregation produces macropores and their subsequent oxidation creates nanopores in the sheets. Different from that in water, the oxidation of FeI_2 in ethanol would proceed as follows.

$$3\ FeI_2 + 2\ O_2 \rightarrow 2\ Fe_3O_4 + 3\ I_2 \quad (6)$$

The existence of metastable Fe_3O_4 may be attributed to the reductive ability of ethanol. In the reaction, part of Fe_3O_4 could be oxidized to α-Fe_2O_3. As the resulting α-Fe_2O_3 is suspended in the ethanol, it can be easily separated from the Fe_3O_4 films. Although surfactants are not required to act as templates for the formation of hierarchical porous structure in our study, their addition would further enhance the corrosion of iron, which seems to favor the formation of sheet-like iron oxides. This point needs further investigation.

Our method has also been applied to fabricate a hierarchical porous cobalt oxide film on cobalt substrate (ESI†). This suggests that our Kirkendall effect-based method may be general to grow hierarchical porous metal oxides on metal substrates without using any templates. We believe that our novel hierarchical porous oxides are ideal candidates for studying the effects of porous structure and morphology on the catalytic efficiency in organic synthesis, photoelectrochemical cells, and environmental catalysis. For instance, the surface morphology of an electrode has a strong influence on its physical and chemical functions in photoelectrochemical processes.

This work was supported by a grant from the Research Grants Council of the Hong Kong Special Administration Region (Project No. 402904).

Lizhi Zhang,*[a] Jimmy C. Yu,*[b] Zhi Zheng[b] and Cheuk Wan Leung[b]
[a]*Key Laboratory of Pesticide & Chemical Biology, Ministry of Education, College of Chemistry, Central China Normal University, Wuhan, 430079, People's Republic of China.*
E-mail: zhanglz@mail.ccnu.edu.cn; Fax: +86 27 6786 7535; Tel: +86 27 6786 7535
[b]*Department of Chemistry, the Chinese University of Hong Kong, Shatin, N. T., Hong Kong. E-mail: jimyu@cuhk.edu.hk; Fax: +852 2603 5057; Tel: +852 2609 6268*

Notes and references

1 (*a*) E. O. Kirkendall, L. Thomassen and C. Upthegrove, *Trans. AIME*, 1939, **133**, 186; (*b*) E. O. Kirkendall, *Trans. AIME*, 1942, **147**, 104; (*c*) A. D. Smigelskas and E. O. Kirkendall, *Trans. AIME*, 1947, **171**, 130.
2 B. Liu and H. C. Zeng, *J. Am. Chem. Soc.*, 2004, **126**, 16744.
3 Y. D. Yin, R. M. Rioux, C. K. Erdonmez, S. Hughes, C. A. Somorjai and A. P. Alivisatos, *Science*, 2004, **304**, 711.
4 N. Uekawa and K. Kaneko, *J. Phys. Chem. B*, 1998, **102**, 8719.
5 M.-O. Coppens, J. H. Sun and T. Maschmeyer, *Catal. Today*, 2001, **69**, 331 and references therein.
6 (*a*) H. F. Zhang, G. C. Hardy, M. J. Rosseinsky and A. I. Cooper, *Adv. Mater.*, 2003, **15**, 78; (*b*) J. El Haskouri, D. O. de Zarate, C. Guillem, A. Beltran-Porter, M. Caldes, M. D. Marcos, D. Beltran-Porter, J. Latorre and P. Amoros, *Chem. Mater.*, 2002, **14**, 4502; (*c*) Y. S. Shin, J. Liu, L. Q. Wang, Z. M. Nie, W. D. Samuels, G. E. Fryxell and G. J. Exarhos, *Angew. Chem. Int. Ed.*, 2000, **39**, 2702; (*d*) K. Nakanishi, Y. Kobayashi, T. Amatani, K. Hirao and T. Kodaira, *Chem. Mater.*, 2004, **16**, 3647; (*e*) Z. Y. Yuan, T. Z. Ren, A. Vantomme and B. L. Su, *Chem. Mater.*, 2004, **16**, 5096.
7 L. Z. Zhang and J. C. Yu, *Chem. Commun.*, 2003, 2078.
8 T. Z. Ren, Z. Y. Yuan and B. L. Su, *Chem. Phys. Lett.*, 2004, **388**, 46.
9 (*a*) V. P. Valtchev, M. Smaihi, A. C. Faust and L. Vidal, *Chem. Mater.*, 2004, **16**, 1350; (*b*) B. J. Zhang, S. A. Davis, N. H. Mendelson and S. Mann, *Chem. Commun.*, 2000, 781; (*c*) M. W. Anderson, S. M. Holmes, N. Hanif and C. S. Cundy, *Angew. Chem. Int. Ed.*, 2000, **39**, 2710.
10 A. Leonard, J. L. Blin and B. L. Su, *Chem. Commun.*, 2003, 2568.
11 A. Taguchi, J. H. Smatt and M. Linden, *Adv. Mater.*, 2003, **15**, 1209.
12 A. V. Neimark, S. Ruetsch, K. G. Kornev and P. I. Ravikovitch, *Nano Lett.*, 2003, **3**, 419.
13 J. S. Sakamoto and B. Dunn, *J. Mater. Chem.*, 2002, **12**, 2859.
14 Y. Ding and J. Erlebacher, *J. Am. Chem. Soc.*, 2003, **125**, 7772.
15 (*a*) J. G. Yu, J. C. Yu, L. Z. Zhang, X. C. Wang and L. Wu, *Chem. Commun.*, 2004, 2414; (*b*) D. Walsh and S. Mann, *Nature*, 1995, **377**, 320.
16 (*a*) J. K. Yuan, K. Laubernds, Q. H. Zhang and S. L. Suib, *J. Am. Chem. Soc.*, 2003, **125**, 4996; (*b*) R. Patrice, L. Dupont, L. Aldon, J.-C. Jumas, E. Wang and J.-M. Tarascon, *Chem. Mater.*, 2004, **16**, 2772.
17 (*a*) Z. Q. Li, Y. Ding, Y. J. Xiong, Q. Yang and Y. Xie, *Chem. Eur. J.*, 2004, **10**, 5823; (*b*) H. Imai, S. Iwai and S. Yamabi, *Chem. Lett.*, 2004, **33**, 768.
18 Z. Y. Yuan, T. Z. Ren and B. L. Su, *Catal. Today*, 2004, **93–95**, 743.
19 O. Shekhah, W. Ranke, A. Schule, G. Kolios and R. Schlogl, *Angew. Chem. Int. Ed.*, 2003, **42**, 5760.
20 (*a*) M. A. Gondal, A. Hameed, Z. H. Yamani and A. Suwaiyan, *Appl. Catal. A-Gen.*, 2004, **268**, 159; (*b*) W. B. Ingler, Jr., J. P. Baltrus and S. U. M. Khan, *J. Am. Chem. Soc.*, 2004, **126**, 10238 and references therein.
21 P. Li, D. E. Miser, S. Rabiei, R. T. Yadav and M. R. Hajaligol, *Appl. Catal. B-Environ.*, 2003, **43**, 151.
22 P. Fabrizioli, T. Burgi and A. Baiker, *J. Catal.*, 2002, **206**, 143.
23 M. Lauwiner, P. Rys and J. Wissmann, *Appl. Catal. A-Gen.*, 1998, **172**, 141.
24 B. M. Weckhuysen, D. J. Wang, M. P. Rosynek and J. H. Lunsford, *Angew. Chem. Int. Ed.*, 1997, **36**, 2374.
25 F. Jiao and P. G. Bruce, *Angew. Chem. Int. Ed.*, 2004, **43**, 5958.
26 (*a*) Q. Tang, W. J. Zhou, J. M. Shen, W. Zhang, L. F. Kong and Y. T. Qian, *Chem. Commun.*, 2004, 712; (*b*) L. Z. Zhang, J. C. Yu, M. S. Mo, L. Wu, Q. Li and K. W. Kwong, *J. Am. Chem. Soc.*, 2004, **126**, 8116; (*c*) L. Z. Zhang, J. C. Yu, M. S. Mo, L. Wu, K. W. Kwong and Q. Li, *Small*, 2005, **1**, 349.
27 N. N. Greenwood and A. Earnshaw, *Chemistry of the Elements*, Second ed., Butterworth-Heinemann, Oxford, 1997.
28 J. C. Wren, G. A. Glowa and J. Merritt, *J. Nucl. Mater.*, 1999, **265**, 161.
29 (*a*) C. R. Wang, K. B. Tang, Q. Yang, G. Z. Shen, B. Hai, C. H. An, J. Zuo and Y. T. Qian, *J. Solid State Chem.*, 2001, **160**, 50; (*b*) C. R. Wang, K. B. Tang, Q. Yang, J. Q. Hu and Y. T. Qian, *J. Mater. Chem.*, 2002, **12**, 2426; (*c*) C. R. Wang, K. B. Tang, Q. Yang, S. H. Lu, G. Zhou, F. Q. Li, W. C. Yu and Y. T. Qian, *J. Cryst. Growth*, 2001, **226**, 175; (*d*) C. R. Wang, Q. Yang, K. B. Tang and Y. T. Qian, *Chem. Lett.*, 2001, 154.